Transverse momentum and collision energy dependence of high p_T hadron suppression in Au+Au collisions at ultrarelativistic energies

J. Adams,[3] C. Adler,[12] M.M. Aggarwal,[25] Z. Ahammed,[28] J. Amonett,[17] B.D. Anderson,[17] M. Anderson,[5] D. Arkhipin,[11] G.S. Averichev,[10] S.K. Badyal,[16] J. Balewski,[13] O. Barannikova,[28,10] L.S. Barnby,[17] J. Baudot,[15] S. Bekele,[24] V.V. Belaga,[10] R. Bellwied,[41] J. Berger,[12] B.I. Bezverkhny,[43] S. Bhardwaj,[29] P. Bhaskar,[38] A.K. Bhati,[25] H. Bichsel,[40] A. Billmeier,[41] L.C. Bland,[2] C.O. Blyth,[3] B.E. Bonner,[30] M. Botje,[23] A. Boucham,[34] A. Brandin,[21] A. Bravar,[2] R.V. Cadman,[1] X.Z. Cai,[33] H. Caines,[43] M. Calderón de la Barca Sánchez,[2] J. Carroll,[18] J. Castillo,[18] M. Castro,[41] D. Cebra,[5] P. Chaloupka,[9] S. Chattopadhyay,[38] H.F. Chen,[32] Y. Chen,[6] S.P. Chernenko,[10] M. Cherney,[8] A. Chikanian,[43] B. Choi,[36] W. Christie,[2] J.P. Coffin,[15] T.M. Cormier,[41] J.G. Cramer,[40] H.J. Crawford,[4] D. Das,[38] S. Das,[38] A.A. Derevschikov,[27] L. Didenko,[2] T. Dietel,[12] X. Dong,[32,18] J.E. Draper,[5] K.A. Drees,[2] F. Du,[43] A.K. Dubey,[14] V.B. Dunin,[10] J.C. Dunlop,[2] M.R. Dutta Majumdar,[38] V. Eckardt,[19] L.G. Efimov,[10] V. Emelianov,[21] J. Engelage,[4] G. Eppley,[30] B. Erazmus,[34] P. Fachini,[2] V. Faine,[2] J. Faivre,[15] R. Fatemi,[13] K. Filimonov,[18] P. Filip,[9] E. Finch,[43] Y. Fisyak,[2] D. Flierl,[12] K.J. Foley,[2] J. Fu,[42] C.A. Gagliardi,[35] M.S. Ganti,[38] N. Gagunashvili,[10] J. Gans,[43] L. Gaudichet,[34] M. Germain,[15] F. Geurts,[30] V. Ghazikhanian,[6] P. Ghosh,[38] J.E. Gonzalez,[6] O. Grachov,[41] V. Grigoriev,[21] S. Gronstal,[8] D. Grosnick,[37] M. Guedon,[15] S.M. Guertin,[6] A. Gupta,[16] E. Gushin,[21] T.D. Gutierrez,[5] T.J. Hallman,[2] D. Hardtke,[18] J.W. Harris,[43] M. Heinz,[43] T.W. Henry,[35] S. Heppelmann,[26] T. Herston,[28] B. Hippolyte,[43] A. Hirsch,[28] E. Hjort,[18] G.W. Hoffmann,[36] M. Horsley,[43] H.Z. Huang,[6] S.L. Huang,[32] T.J. Humanic,[24] G. Igo,[6] A. Ishihara,[36] P. Jacobs,[18] W.W. Jacobs,[13] M. Janik,[39] I. Johnson,[18] P.G. Jones,[3] E.G. Judd,[4] S. Kabana,[43] M. Kaneta,[18] M. Kaplan,[7] D. Keane,[17] J. Kiryluk,[6] A. Kisiel,[39] J. Klay,[18] S.R. Klein,[18] A. Klyachko,[13] D.D. Koetke,[37] T. Kollegger,[12] A.S. Konstantinov,[27] M. Kopytine,[17] L. Kotchenda,[21] A.D. Kovalenko,[10] M. Kramer,[22] P. Kravtsov,[21] K. Krueger,[1] C. Kuhn,[15] A.I. Kulikov,[10] A. Kumar,[25] G.J. Kunde,[43] C.L. Kunz,[7] R.Kh. Kutuev,[11] A.A. Kuznetsov,[10] M.A.C. Lamont,[3] J.M. Landgraf,[2] S. Lange,[12] C.P. Lansdell,[36] B. Lasiuk,[43] F. Laue,[2] J. Lauret,[2] A. Lebedev,[2] R. Lednický,[10] V.M. Leontiev,[27] M.J. LeVine,[2] C. Li,[32] Q. Li,[41] S.J. Lindenbaum,[22] M.A. Lisa,[24] F. Liu,[42] L. Liu,[42] Z. Liu,[42] Q.J. Liu,[40] T. Ljubicic,[2] W.J. Llope,[30] H. Long,[6] R.S. Longacre,[2] M. Lopez-Noriega,[24] W.A. Love,[2] T. Ludlam,[2] D. Lynn,[2] J. Ma,[6] Y.G. Ma,[33] D. Magestro,[24] S. Mahajan,[16] L.K. Mangotra,[16] D.P. Mahapatra,[14] R. Majka,[43] R. Manweiler,[37] S. Margetis,[17] C. Markert,[43] L. Martin,[34] J. Marx,[18] H.S. Matis,[18] Yu.A. Matulenko,[27] T.S. McShane,[8] F. Meissner,[18] Yu. Melnick,[27] A. Meschanin,[27] M. Messer,[2] M.L. Miller,[43] Z. Milosevich,[7] N.G. Minaev,[27] C. Mironov,[17] D. Mishra,[14] J. Mitchell,[30] B. Mohanty,[38] L. Molnar,[28] C.F. Moore,[36] M.J. Mora-Corral,[19] V. Morozov,[18] M.M. de Moura,[41] M.G. Munhoz,[31] B.K. Nandi,[38] S.K. Nayak,[16] T.K. Nayak,[38] J.M. Nelson,[3] P. Nevski,[2] V.A. Nikitin,[11] L.V. Nogach,[27] B. Norman,[17] S.B. Nurushev,[27] G. Odyniec,[18] A. Ogawa,[2] V. Okorokov,[21] M. Oldenburg,[18] D. Olson,[18] G. Paic,[24] S.U. Pandey,[41] S.K. Pal,[38] Y. Panebratsev,[10] S.Y. Panitkin,[2] A.I. Pavlinov,[41] T. Pawlak,[39] V. Perevoztchikov,[2] W. Peryt,[39] V.A. Petrov,[11] S.C. Phatak,[14] R. Picha,[5] M. Planinic,[44] J. Pluta,[39] N. Porile,[28] J. Porter,[2] A.M. Poskanzer,[18] M. Potekhin,[2] E. Potrebenikova,[10] B.V.K.S. Potukuchi,[16] D. Prindle,[40] C. Pruneau,[41] J. Putschke,[19] G. Rai,[18] G. Rakness,[13] R. Raniwala,[29] S. Raniwala,[29] O. Ravel,[34] R.L. Ray,[36] S.V. Razin,[10,13] D. Reichhold,[28] J.G. Reid,[40] G. Renault,[34] F. Retiere,[18] A. Ridiger,[21] H.G. Ritter,[18] J.B. Roberts,[30] O.V. Rogachevski,[10] J.L. Romero,[5] A. Rose,[41] C. Roy,[34] L.J. Ruan,[32,2] V. Rykov,[41] R. Sahoo,[14] I. Sakrejda,[18] S. Salur,[43] J. Sandweiss,[43] I. Savin,[11] J. Schambach,[36] R.P. Scharenberg,[28] N. Schmitz,[19] L.S. Schroeder,[18] K. Schweda,[18] J. Seger,[8] D. Seliverstov,[21] P. Seyboth,[19] E. Shahaliev,[10] M. Shao,[32] M. Sharma,[25] K.E. Shestermanov,[27] S.S. Shimanskii,[10] R.N. Singaraju,[38] F. Simon,[19] G. Skoro,[10] N. Smirnov,[43] R. Snellings,[23] G. Sood,[25] P. Sorensen,[6] J. Sowinski,[13] H.M. Spinka,[1] B. Srivastava,[28] S. Stanislaus,[37] R. Stock,[12] A. Stolpovsky,[41] M. Strikhanov,[21] B. Stringfellow,[28] C. Struck,[12] A.A.P. Suaide,[41] E. Sugarbaker,[24] C. Suire,[2] M. Šumbera,[9] B. Surrow,[2] T.J.M. Symons,[18] A. Szanto de Toledo,[31] P. Szarwas,[39] A. Tai,[6] J. Takahashi,[31] A.H. Tang,[2,23] D. Thein,[6] J.H. Thomas,[18] V. Tikhomirov,[21] M. Tokarev,[10] M.B. Tonjes,[20] T.A. Trainor,[40] S. Trentalange,[6] R.E. Tribble,[35] M.D. Trivedi,[38] V. Trofimov,[21] O. Tsai,[6] T. Ullrich,[2] D.G. Underwood,[1] G. Van Buren,[2] A.M. VanderMolen,[20] A.N. Vasiliev,[27] M. Vasiliev,[35] S.E. Vigdor,[13] Y.P. Viyogi,[38] S.A. Voloshin,[41] W. Waggoner,[8] F. Wang,[28] G. Wang,[17] X.L. Wang,[32] Z.M. Wang,[32] H. Ward,[36] J.W. Watson,[17] R. Wells,[24] G.D. Westfall,[20] C. Whitten Jr.,[6] H. Wieman,[18] R. Willson,[24] S.W. Wissink,[13] R. Witt,[43] J. Wood,[6] J. Wu,[32] N. Xu,[18] Z. Xu,[2] Z.Z. Xu,[32] A.E. Yakutin,[27] E. Yamamoto,[18] J. Yang,[6] P. Yepes,[30] V.I. Yurevich,[10] Y.V. Zanevski,[10] I. Zborovský,[9] H. Zhang,[43,2] H.Y. Zhang,[17]

W.M. Zhang,[17] Z.P. Zhang,[32] P.A. Żołnierczuk,[13] R. Zoulkarneev,[11] J. Zoulkarneeva,[11] and A.N. Zubarev[10]

(STAR Collaboration),[*]

[1]*Argonne National Laboratory, Argonne, Illinois 60439*
[2]*Brookhaven National Laboratory, Upton, New York 11973*
[3]*University of Birmingham, Birmingham, United Kingdom*
[4]*University of California, Berkeley, California 94720*
[5]*University of California, Davis, California 95616*
[6]*University of California, Los Angeles, California 90095*
[7]*Carnegie Mellon University, Pittsburgh, Pennsylvania 15213*
[8]*Creighton University, Omaha, Nebraska 68178*
[9]*Nuclear Physics Institute AS CR, Řež/Prague, Czech Republic*
[10]*Laboratory for High Energy (JINR), Dubna, Russia*
[11]*Particle Physics Laboratory (JINR), Dubna, Russia*
[12]*University of Frankfurt, Frankfurt, Germany*
[13]*Insitute of Physics, Bloomington, Indiana 47408*
[14]*Insitute of Physics, Bhubaneswar 751005, India*
[15]*Institut de Recherches Subatomiques, Strasbourg, France*
[16]*University of Jammu, Jammu 180001, India*
[17]*Kent State University, Kent, Ohio 44242*
[18]*Lawrence Berkeley National Laboratory, Berkeley, California 94720*
[19]*Max-Planck-Institut für Physik, Munich, Germany*
[20]*Michigan State University, East Lansing, Michigan 48824*
[21]*Moscow Engineering Physics Institute, Moscow Russia*
[22]*City College of New York, New York City, New York 10031*
[23]*NIKHEF, Amsterdam, The Netherlands*
[24]*Ohio State University, Columbus, Ohio 43210*
[25]*Panjab University, Chandigarh 160014, India*
[26]*Pennsylvania State University, University Park, Pennsylvania 16802*
[27]*Institute of High Energy Physics, Protvino, Russia*
[28]*Purdue University, West Lafayette, Indiana 47907*
[29]*University of Rajasthan, Jaipur 302004, India*
[30]*Rice University, Houston, Texas 77251*
[31]*Universidade de Sao Paulo, Sao Paulo, Brazil*
[32]*University of Science & Technology of China, Anhui 230027, China*
[33]*Shanghai Institute of Nuclear Research, Shanghai 201800, P.R. China*
[34]*SUBATECH, Nantes, France*
[35]*Texas A & M, College Station, Texas 77843*
[36]*University of Texas, Austin, Texas 78712*
[37]*Valparaiso University, Valparaiso, Indiana 46383*
[38]*Variable Energy Cyclotron Centre, Kolkata 700064, India*
[39]*Warsaw University of Technology, Warsaw, Poland*
[40]*University of Washington, Seattle, Washington 98195*
[41]*Wayne State University, Detroit, Michigan 48201*
[42]*Institute of Particle Physics, CCNU (HZNU), Wuhan, 430079 China*
[43]*Yale University, New Haven, Connecticut 06520*
[44]*University of Zagreb, Zagreb, HR-10002, Croatia*
(Dated: September 2, 2003)

We report high statistics measurements of inclusive charged hadron production in Au+Au and p+p collisions at $\sqrt{s_{\mathrm{NN}}}$=200 GeV. A large, approximately constant hadron suppression is observed in central Au+Au collisions for 5<p_T<12 GeV/c. The collision energy dependence of the yields and the centrality and p_T dependence of the suppression provide stringent constraints on theoretical models of suppression. Models incorporating initial-state gluon saturation or partonic energy loss in dense matter are largely consistent with observations. We observe no evidence of p_T-dependent suppression, which may be expected from models incorporating jet attentuation in cold nuclear matter or scattering of fragmentation hadrons.

High energy partons propagating through matter are predicted to lose energy via induced gluon radiation, with the total energy loss strongly dependent on the color charge density of the medium [1]. This process can provide a sensitive probe of the hot and dense matter generated early in ultrarelativistic nuclear collisions, when a

plasma of deconfined quarks and gluons may form. The hard scattering and subsequent fragmentation of partons originating from the incoming nuclei generates jets of correlated hadrons. In nuclear collisions, jets may be studied via observables such as high transverse momentum (high p_T) hadronic inclusive spectra [2] and correlations. Several striking high p_T phenomena have been observed at the Relativistic Heavy Ion Collider (RHIC) [3, 4, 5, 6, 7], including strong suppression of inclusive hadron production in the most central, violent nuclear interactions [3, 4, 5]. These phenomena are consistent with large partonic energy loss in high energy density matter [1, 8, 9, 10, 11] though other mechanisms have also been proposed to account for the existing data, including gluon saturation in the initial nuclear wavefunction [12], attenuation of jet formation in cold nuclear matter [13], and scattering of fragmentation hadrons [14]. Additional measurements are required to discriminate among these pictures and to isolate effects due to final state partonic energy loss.

We report high statistics measurements of the inclusive charged hadron yield $(h^+ + h^-)/2$ (defined as the summed yields of primary $\pi^\pm$, $K^\pm$, p and $\bar{p}$) for $0.2 < p_T < 12$ GeV/c in Au+Au collisions and $0.4 < p_T < 10$ GeV/c in non-singly diffractive (NSD) p+p collisions at nucleon-nucleon center of mass energy $\sqrt{s_{NN}}=200$ GeV. The Au+Au data extend considerably the p_T range of earlier charged hadron suppression studies, and the p+p data are the first such measurement at this energy. Comparisons are made to several theoretical models. The high precision and broad kinematic coverage of the data significantly constrain the possible mechanisms of hadron suppression. In addition, the energy dependence of the yields may be sensitive to gluon shadowing at low Bjorken x in heavy nuclei.

We compare the data to two calculations based on hard parton scattering evaluated via perturbative QCD (pQCD-I [15] and pQCD-II [9]) and to a calculation extending the saturation model to high momentum transfer [12]. Both pQCD models for Au+Au collisions incorporate nuclear shadowing of initial-state parton densities, the Cronin effect [16], and partonic energy loss, but with different formulations. pQCD-I results excluding one or more nuclear effects are also shown, to illustrate sensitivity to such effects. Neither pQCD calculation includes non-perturbative effects that generate particle species-dependent differences for $p_T < 5$ GeV/c[15, 17].

The Au+Au and p+p data were recorded by the STAR collaboration during the first $\sqrt{s_{NN}}=200$ GeV runs at RHIC. Charged particle trajectories were measured in the Time Projection Chamber (TPC) [18]. The solenoidal magnetic field was 0.5 T, resulting in a factor of three improvement in momentum resolution at high p_T relative to [3, 6].

After event selection cuts, the Au+Au dataset comprised 1.7 million minimum bias events ($97 \pm 3\%$ of the

TABLE I: Multiplicative correction factors applied to the measured yields at $p_T=10$ GeV/c for p+p and Au+Au data. Factors vary by approximately 5% for $4 < p_T < 12$ GeV/c and have similar uncertainties.

	Tracking	Background	p_T resolution
p+p	1.18 ± 0.07	0.90 ± 0.08	$0.89\ ^{+0.05}_{-0.05}$
Au+Au 60-80%	1.11 ± 0.06	0.95 ± 0.05	$0.97\ ^{+0.03}_{-0.05}$
Au+Au 0-5%	1.25 ± 0.06	0.94 ± 0.06	$0.95\ ^{+0.05}_{-0.05}$

geometric cross section σ^{AuAu}_{geom}) and 1.5 million central events (10% of σ^{AuAu}_{geom}). Centrality selection and analysis of spectra follow Ref. [3]. Background at high p_T is dominated by weak decay products, with correction factors calculated using STAR measurements of $\Lambda(+\Sigma^0)$ and K^0_s for $p_T < 6$ GeV/c [19] and assuming constant yield ratios $\Lambda(+\Sigma^0)/(h^+ + h^-)$ and $K^0_s/(h^+ + h^-)$ for $p_T > 6$ GeV/c. The $\Lambda(+\Sigma^0)$ yield was scaled by a factor 1.4 to account for Σ^+ decays. Background due to other sources is negligible. Table I summarizes the correction factors at high p_T.

After event selection cuts, the p+p dataset comprised 5 million mainly NSD events, triggered on the coincidence of two Beam-Beam counters (BBCs). The BBCs are annular scintillator detectors situated ± 3.5 m from the interaction region, covering pseudorapidity $3.3 < |\eta| < 5.0$. A van der Meer scan [20] measured the BBC trigger cross section to be $26.1 \pm 0.2(\text{stat}) \pm 1.8(\text{sys})$ mb. The BBC trigger was simulated using PYTHIA [21] and HERWIG [22] events passed though a GEANT detector model. The PYTHIA trigger cross section is 27 mb, consistent with measurement, of which 0.7 mb results from singly diffractive events. The PYTHIA and HERWIG simulations show that the trigger accepts $87 \pm 8\%$ of all NSD events containing a TPC track, with negligible track p_T-dependence. Non-interaction backgrounds contributed $3 \pm 2\%$ of the trigger rate.

The high p+p interaction rate generated significant pileup in the TPC. Valid tracks matched an in-time hit in the Central Trigger Barrel (CTB [18]) surrounding the TPC and projected to a distance of closest approach $DCA < 1$ cm to the average beam trajectory. To avoid event selection multiplicity bias, an approximate event vertex position along the beam (z_{vert}) was calculated by averaging z_{DCA} over all valid tracks. Accepted events were required to have $|z_{vert}| < 75$ cm, corresponding to $69 \pm 4\%$ of all events. The track momentum fit did not include the event vertex. The CTB track-matching efficiency is $94 \pm 2\%$ and combinatorial background is $2 \pm 2\%$. Other significant p+p tracking backgrounds result from weak decays and from antinucleon annihilation in detector material, with corrections calculated using HIJING [23] and preliminary STAR measurements. Tracking correction factors at high p_T are given in Table I. For p+p collisions relative to peripheral Au+Au, exclusion of the
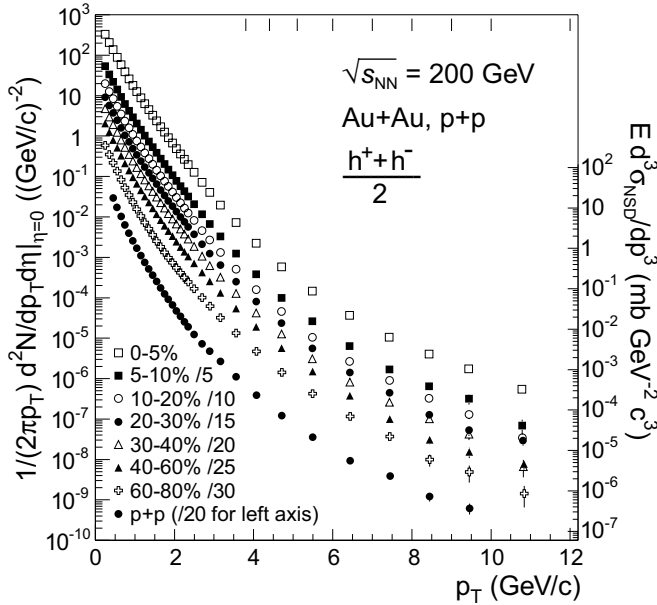
FIG. 1: Inclusive invariant p_T distributions of $(h^+ + h^-)/2$ for centrality-selected Au+Au and p+p NSD interactions. Hash marks at the top indicate bin boundaries for $p_T > 4$ GeV/c. The invariant cross section for p+p is indicated on right vertical axis.
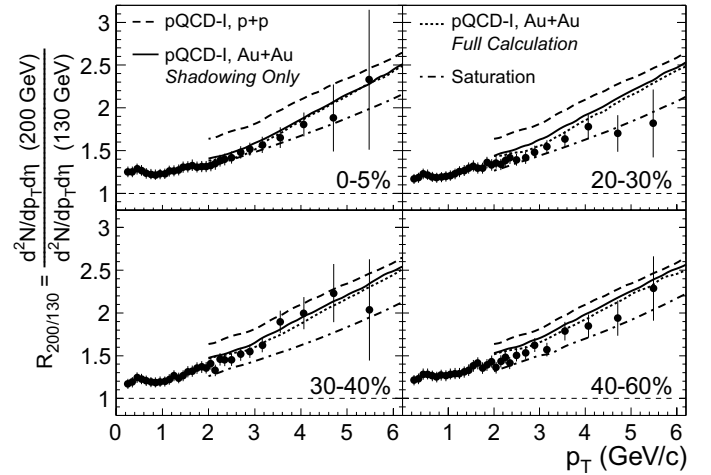

FIG. 2: $R_{200/130}(p_T)$ vs. p_T for $(h^+ + h^-)/2$ for four different centrality bins. Error bars show statistical and systematic uncertainties. The overall normalization uncertainty is $^{+6}_{-10}\%$ for the 40-60% bin and is negligible for the other panels. Calculations are described in the text.

event vertex from the momentum fit results in poorer p_T resolution, while the CTB matching requirement results in lower tracking efficiency. The p+p inclusive spectrum was also analysed for $p_T < 3.5$ GeV/c by an independent method in which a primary vertex is found and incorporated into the track fit, with the result consistent within uncertainties with the spectrum reported here.

The p+p NSD differential cross section is the product of the measured per-event yield and the BBC NSD trigger cross section, and has a normalization uncertainty of ±14%. The charged hadron invariant cross section has been measured in $\bar{p} + p$ collisions at $\sqrt{s}$=200 GeV [24]. The p+p cross section reported here is smaller by a factor of 0.79 ± 0.18, approximately independent of p_T, where the uncertainty includes the two spectrum normalizations and the correction for different acceptances [3]. The difference is due in large part to differing NSD cross section, which is 35 ± 1 mb in [24] but is measured here to be 30.0 ± 3.5 mb.

Figure 1 shows inclusive invariant p_T distributions of $(h^+ + h^-)/2$ within $|\eta| < 0.5$ for Au+Au and p+p collisions at $\sqrt{s_{NN}}$=200 GeV. The centrality-selected Au+Au spectra are shown for percentiles of σ^{AuAu}_{geom}, with 0-5% indicating the most central (head-on) collisions. Error bars are the quadrature sum of the statistical error and the systematic uncertainty and are dominated by the latter except at the highest p_T.

Figure 2 shows $R_{200/130}(p_T)$, the ratio of charged hadron yields at $\sqrt{s_{NN}}$=200 and 130 GeV[3], for central-ity selected Au+Au collisions. Error bars are the quadrature sum of the statistical and systematic uncertainties, dominated for $p_T > 4$ GeV/c by statistics at 130 GeV. In the absence of nuclear effects, the hard process inclusive yield in nuclear collisions is expected to scale as $\langle N_{bin} \rangle$, the average number of binary collisions for the respective centrality selection. $R_{200/130}(p_T)$ has not been scaled by the ratio $N_{bin}(200)/N_{bin}(130)$, which Glauber model calculations [3, 25] give as ~ 1.02 for all centralities.

Figure 2 also shows the saturation model calculation (dot-dashed) and pQCD-I calculations for p+p (dashed) and centrality-selected Au+Au collisions (shadowing-only and full, shown as solid and dotted respectively). Both models approximately reproduce the p_T-dependence of the ratio for Au+Au for $p_T > 2$ GeV/c, with pQCD-I slightly better for more peripheral collisions. The various pQCD-I calculations shown illustrate that in this model the reduction in $R_{200/130}(p_T)$ for Au+Au relative to p+p is predominantly due to nuclear shadowing[15]. This sensitivity arises because the shadowing is x-dependent and at fixed p_T, different $\sqrt{s}$ corresponds to different $x_T = 2p_T/\sqrt{s}$. The quantitative agreement of pQCD-I with the data improves for more peripheral collisions, suggesting that the prescription for the centrality dependence of shadowing in [15] may not be optimal. Alternatively, introduction of $\sqrt{s}$-dependent energy loss to the model in [15] may also improve the agreement.

Modification of inclusive spectra by nuclear effects is measured by comparison to a nucleon-nucleon (NN) reference via the nuclear modification factor:

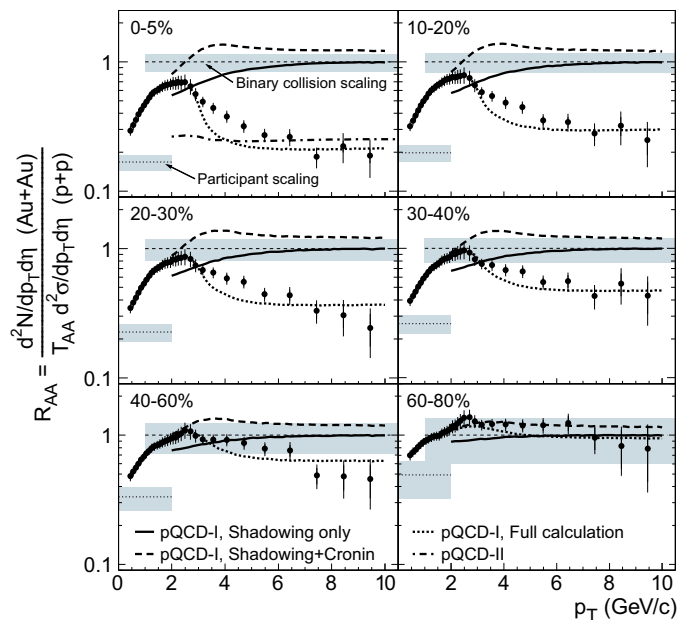$$R_{AA}(p_T) = \frac{d^2N^{AA}/dp_T d\eta}{T_{AA}d^2\sigma^{NN}/dp_T d\eta} , \qquad (1)$$

FIG. 3: $R_{AA}(p_T)$ (Eq. 1) for $(h^+ + h^-)/2$ in $|\eta|$<0.5, for centrality-selected Au+Au spectra relative to the measured p+p spectrum. The p+p spectrum is common to all panels. Error bars include both statistical and systematic uncertainties. Calculations are described in the text.

where $T_{AA}=\langle N_{bin}\rangle/\sigma_{inel}^{NN}$ from a Glauber calculation accounts for the nuclear collision geometry [3, 25] and we adopt $\sigma_{inel}^{NN} = 42$ mb. $d^2\sigma^{NN}/dp_T d\eta$ refers to inelastic collisions, whereas we have measured the p+p NSD differential cross section. However, singly diffractive interactions contribute predominantly to low p_T [26]. A multiplicative correction based on PYTHIA, applied to $d^2\sigma^{NN}/dp_T d\eta$ in Eq. 1, is 1.05 at p_T=0.4 GeV/c and unity above 1.2 GeV/c.

Figure 3 shows $R_{AA}(p_T)$ at $\sqrt{s_{NN}}$=200 GeV for centrality-selected Au+Au spectra relative to the measured p+p spectrum. The horizontal dashed lines show Glauber model expectations [3, 25] for scaling of the yield with $\langle N_{bin}\rangle$ or mean number of participants $\langle N_{part}\rangle$, with the grey bands showing their respective uncertainties summed in quadrature with the p+p normalization uncertainty. The error bars represent the quadrature sum of the Au+Au and remaining p+p spectrum uncertainties. For p_T<6 GeV/c, $R_{AA}(p_T)$ is similar to that observed at $\sqrt{s_{NN}}$=130 GeV [3], though in the present case the reference and Au+Au spectra are measured at the same energy and acceptance. Hadron production for $6<p_T<10$ GeV/c is suppressed by a factor of 4-5 in central Au+Au relative to p+p collisions.

Figure 3 shows the full pQCD-I calculation and the influence of each nuclear effect. The energy loss for central collisions is a fit parameter, with the p_T and centrality dependence of the suppression then constrained by the theory. The Cronin enhancement and shadowing alone
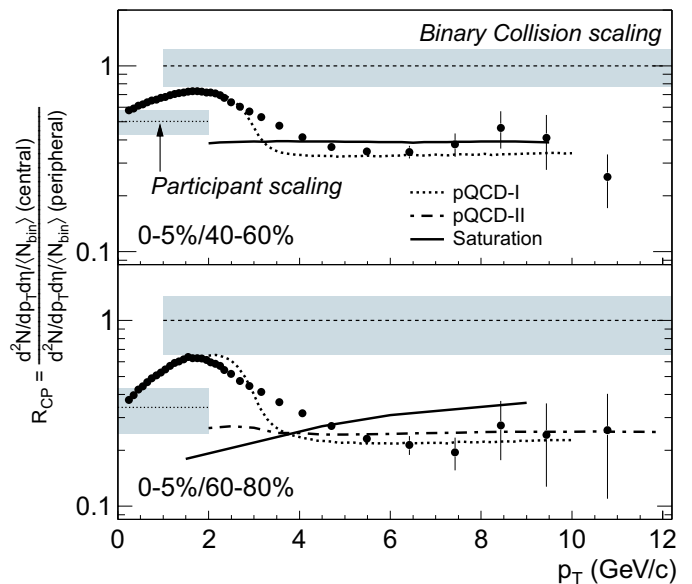

FIG. 4: $R_{CP}(p_T)$ vs. p_T for $(h^+ + h^-)/2$. Error bars include both statistical and systematic uncertainties. Calculations are described in the text.

cannot account for the large suppression, which is reproduced only if partonic energy loss in dense matter is included. The full calculation generally agrees with data for p_T>5 GeV/c if the initial parton density in central collisions is adjusted to be ~15 times that of cold nuclear matter [27]. pQCD-II exhibits similar agreement for central collisions. In Ref. [9], the pQCD-II calculation was used to predict a p_T-independent suppression factor in this p_T range from the interplay between shadowing, the Cronin effect, and partonic energy loss.

Figure 4 shows $R_{CP}(p_T)$, the $\langle N_{bin}\rangle$-normalized ratio of central and peripheral Au+Au spectra. $R_{CP}(p_T)$ extends to higher p_T than $R_{AA}(p_T)$, with smaller point-to-point uncertainties. The error bars show the quadrature sum of statistical and uncorrelated systematic uncertainties. Statistical error of the peripheral spectrum dominates the uncertainties for p_T>8 GeV/c. Dashed lines indicate $\langle N_{bin}\rangle$ and $\langle N_{part}\rangle$ scaling, and the grey bands indicate their uncertainties.

$R_{CP}(p_T)$ for p_T<6 GeV/c is similar to measurements at $\sqrt{s_{NN}}$=130 GeV [3], but is now seen to be approximately constant for $5<p_T<12$ GeV/c. It is consistent with $\langle N_{part}\rangle$ scaling at $p_T \sim 4$ GeV/c as reported in [5], but is below $\langle N_{part}\rangle$ scaling at higher p_T.

The p_T-dependence of the suppression in Figure 4 is well reproduced for p_T>5 GeV/c by the full pQCD-I and pQCD-II calculations in both panels and the saturation calculation in the upper but not the lower panel. The magnitude of suppression is fitted to the central collision data in the pQCD models but is predicted in the saturation calculation. Attenuation of initial jet formation due to multiple nucleon interactions [13] generates

an increase in partonic $R_{AA}(p_T)$ for central collisions of a factor ~ 2 in $5 < E_T < 12$ GeV. Though the model does not incorporate fragmentation, a similar p_T-dependence would be expected for high p_T hadrons, in contrast to observations. Suppression in the final state due to in-medium scattering of fragmentation hadrons should also result in a rising $R_{AA}(p_T)$ with increasing p_T due to the dependence of hadron formation time on the total jet energy [14], though detailed comparison of this model to data requires further theoretical development.

In summary, STAR has measured inclusive charged hadron yields from Au+Au and p+p collisions at $\sqrt{s_{NN}}=200$ GeV, at higher precision and over a much broader p_T range than previous measurements. Large, constant hadron suppression is observed in central nuclear collisions at high p_T. The systematic behaviour of the suppression at high p_T is well described both by pQCD calculations incorporating final-state partonic energy loss in dense matter and a model of initial-state gluon saturation, though the latter model provides a poorer description of peripheral collision data. The isolation of initial state effects on high p_T hadron production may be achieved through the study of d+Au collisions at RHIC, allowing a quantitative measurement of final state effects from the data presented here.

* URL: www.star.bnl.gov

[1] R. Baier, D. Schiff and B.G. Zakharov, Ann. Rev. Nucl. Part. Sci. **50**, 37 (2000); M. Gyulassy, I. Vitev, X.N. Wang, B. Zhang, nucl-th/0302077.

[2] X.N. Wang and M. Gyulassy, Phys. Rev. Lett. **68**, 1480 (1992).

[3] C. Adler *et al.*, Phys. Rev. Lett. **89**, 202301 (2002).

[4] K. Adcox *et al.*, Phys. Rev. Lett. **88**; 022301 (2002); Phys. Lett. **B561**, 82 (2003); S.S. Adler *et al.*, Phys. Rev. Lett. **91**, 072301 (2003).

[5] B.B. Back *et al.*, nucl-ex/0302015.

[6] C. Adler *et al.*, Phys. Rev. Lett. **90**, 032301 (2003).

[7] C. Adler *et al.*, Phys. Rev. Lett. **90**, 082302 (2003).

[8] M. Gyulassy and X.N. Wang, Nucl. Phys. **B420**, 583 (1994); X.N. Wang, Phys. Rev. **C58**, 2321 (1998).

[9] I. Vitev and M. Gyulassy, Phys. Rev. Lett. **89**, 252301 (2002).

[10] C.A. Salgado and U.A. Wiedemann, Phys. Rev. Lett. **89**, 092303 (2002).

[11] T. Hirano and Y. Nara, nucl-th/0301042.

[12] D. Kharzeev, E. Levin and L. McLerran, Phys. Lett. **B561**, 93 (2003); D. Kharzeev, private communication.

[13] R. Lietava, J. Pisut, N. Pisutova, B. Tomasik, Eur. Phys. J. **C28**, 119 (2003).

[14] K. Gallmeister, C. Greiner and Z. Xu, Phys. Rev. **C67**, 044905 (2003). Note that Eq. (2) of this reference implies that $\langle L/\lambda \rangle$ in Fig. 9 decreases substantially in $5 < p_T < 12$ GeV/c.

[15] X.N. Wang, nucl-th/0305010; private communication. Calculations use model parameters $\mu_0 = 2.0$ GeV and $\epsilon_0 = 2.04$ GeV/fm.

[16] D. Antreasyan *et al.*, Phys. Rev. **D19**, 764 (1979); P.B. Straub *et al.*, Phys. Rev. Lett. **68**, 452 (1992).

[17] I. Vitev and M. Gyulassy, Phys. Rev. **C65**, 041902 (2002); R.J. Fries, B. Muller, C. Nonaka and S.A. Bass, Phys. Rev. Lett. **90** 202303 (2003).

[18] M. Anderson *et al.*, Nucl. Instr. Meth. **A499**, 659 (2003).

[19] J. Adams *et al.*, nucl-ex/0306007.

[20] A. Drees and Z. Xu, Proceedings of the Particle Accelerator Conference 2001, Chicago, Il, p. 3120.

[21] T. Sjoestrand *et al.*, Comp. Phys. Comm. **135**, 238 (2001).

[22] G. Corcella *et al.*, JHEP **0101**, 010 (2001).

[23] X.N. Wang and M. Gyulassy, Phys. Rev. **D44**, 3501 (1991).

[24] C. Albajar *et al.*, Nucl. Phys. **B335**, 261 (1990).

[25] Correction for a recently found error in the Glauber calculation reported in [3] yields $\sim$2-6% larger $\langle N_{bin} \rangle$ values, with the largest increase for the most peripheral and central bins. Negligible change results for $\langle N_{part} \rangle$. We thank K. Reygers for valuable discussions.

[26] M. Derrick *et al.*, Z. Phys. **C67**, 227 (1995); R.E. Ansorge *et al.*, Z. Phys. **C33**, 175 (1986).

[27] E. Wang and X.N. Wang, Phys. Rev. Lett. **89**, 162301 (2002); F. Arleo, Phys. Lett. **B532**, 231 (2002).